

ScS₂ Monolayer as a Potential Cathode Material for Alkali-ion Batteries and Beyond

Dwaipayan Chakraborty,* Madhu Pandey, and Priya Johari*

*Department of Physics, School of Natural Sciences, Shiv Nadar University, Greater Noida,
Gautam Buddha Nagar, U.P. (India) – 201314*

E-mail: dc167@snu.edu.in; priya.johari@snu.edu.in

2D materials, transition metal dichalcogenides, ScS₂ monolayer, cathode materials, open circuit voltage gravimetric capacity, diffusion kinetics

Introduction:

With the decreasing stock of fossil fuels and increasing environmental pollution, the demand for green energy sources and rechargeable energy storage devices in recent times is like never before. Lithium-ion batteries (LIBs) have been in the forefront of the secondary battery technology since its first commercialization in 1991¹. LIBs are known to deliver high energy density, high reversible capacity, excellent cycling stability, and to have relatively simple reaction mechanism due to which they are being widely used in portable electronic devices and in recent time, in electric vehicles^{2,3}. However, limited lithium resources in highly localized manner in few geographical locations and the water extensive mining processes hinder the cost effectiveness of LIBs and create environmental concerns. Along with this there are also intrinsic safety issues with LIBs. All of these drawbacks collectively push to search for other metal-ion batteries^{4,5}. In this context sodium-ion batteries (NIBs), potassium-ion batteries (KIBs), magnesium-ion batteries and aluminum-ion batteries have gained huge research interests in recent times due to relatively higher abundance of these metals in the earth's crust.

Any metal-ion battery has main three components namely anode, electrolyte and cathode among which cathode is the most expensive and has largest weight, and thus, controls the cost and the specific capacity of the battery to a large extent³. Therefore, developing high energy high power cathode materials for LIBs and non-LIBs is a key challenge. However, LiCoO₂, the most popular cathode material in commercial LIBs delivers specific capacity around 140 mA h g⁻¹ only⁶. Other layered oxide materials like LiMnO₂, LiNi_{0.5}Mn_{0.5}O₂ also struggle to cross 200 mA h g⁻¹ specific capacity³. On the other hand, the olivine LiFePO₄ has also been reported to deliver the specific capacity ~140 mA h g⁻¹ only with better cycling

stability⁷. The same situation can be evidenced for NIBs also. Layered cathode materials like NaMO₂ (M = Mn, Ni, Co) and their derivatives can only deliver theoretical capacities around 250 mA h g⁻¹⁸. Polyanionic compounds like NaFePO₄, Na₃V₂(PO₄)₃ deliver even less theoretical capacity of 154 mA h g⁻¹ and 117 mA h g⁻¹, respectively⁸.

Also the preparation of well-ordered bulk structures are difficult and layered materials suffer from capacity fading in the bulk form⁹. In this context, due to relatively low weight, large surface to volume ratio, good conductivity on the surface, mechanical stability etc., several 2D materials have gained huge scientific attention for their exploration as new generation electrode materials. Although graphene is not an ideal electrode for LIBs¹⁰ but other graphene-like 2D materials such as silicene¹¹, germanene¹², borophene¹³ and phosphorene^{14,15} have been shown to deliver high specific capacity when used as anode. Numerous other 2D materials explored mainly as anode like metal oxides and metal nitrides¹⁶, transition-metal dichalcogenides (TMDCs)¹⁷, MXenes¹⁷ exhibit promising electrochemical performances with large specific capacities, high rate capabilities, and good cycling stabilities. On the cathode side a few 2D materials like MoN₂², MnO₂, CoO₂, NiO₂⁹, ScO₂¹⁸, V₂O₅ monolayer¹⁹, NbS₂²⁰ for alkali-ion batteries, MoS₂ nanoribbon for Mg-ion batteries²¹ etc. have been theoretically studied in the recent times.

Inspired from these studies and the fact that Sc is the lightest transition metal which could help to achieve the goal of high theoretical capacity, we here explored the performance of ScS₂ monolayer as a cathode material for alkali-ion batteries (Li, Na, K) and other multi-valent metal-ion batteries (Mg, Al). Previous studies on ScS₂ have focused only on the fundamental electronic and magnetic properties of the ScS₂ monolayer, but not on its possible applications^{22,23}. Our first-principles calculations show that 2D ScS₂ is able to deliver large theoretical capacity of 491.36 mA h g⁻¹ for alkali-ions and 324.29 mA h g⁻¹ for Mg and Al-ions while maintaining good average open-circuit voltages. We also studied the diffusivity of these metal-ions on the ScS₂ surface which is related to the charge/discharge rate capability of batteries. Our results suggest low diffusion barriers for all metal-ions except Al.

Owing to these results, we therefore believe that the ScS₂ monolayer can be an interesting candidate for cathode material to be used in alkali-ion batteries and beyond.

Computational Details:

We employed the first-principles calculations in the framework of the density functional theory (DFT) as implemented in the VASP (Vienna ab initio simulation package)^{24–26} package to study the performance of ScS₂ monolayer as cathode for metal-ion (Li, Na, K, Mg, Al) batteries. We used the projector augmented-wave (PAW) pseudopotentials²⁷ to treat the electron-ion interactions with a plane-wave cutoff energy of 400 eV. The electron-electron exchange correlation was described by the generalized gradient approximation (GGA) within the Perdew–Burke–Ernzerhof²⁸ formalism. We also incorporated the vdW effect in our adsorption calculations by considering the DFT-D3 method of Grimme²⁹ for empirical dispersion corrections. The energy and the Hellmann–Feynman force convergence criteria of 10⁻⁴ eV and 0.01 eV/Å, respectively were used for all the calculations. We introduced a vacuum of ~25 Å between the two layers of ScS₂ to avoid any interaction with the periodic image in that direction in order to realize the monolayer. A 3×3×1 supercell was considered to study the adsorption of the metal atoms so that the change in the binding energy and average open circuit voltage (OCV) with the concentration of adatoms can be studied in detail. For geometry optimization of the absorbed system 6×6×1 *k*-points were considered for the Brillouin zone integration within the Monkhorst–Pack scheme³⁰. To study the diffusion of a single metal atom on the ScS₂ surface we employed the climbing-image nudged elastic band (CI-NEB) method³¹. In this method the images initially defined by the linear interpolation between the two minima are relaxed to define a minimum energy path (MEP). DFT computes the forces both on the images and the elastic band. The MEP is defined when the component of the force not pointing along the path direction defined by the images is zero. We considered the force convergence criteria for the CI-NEB calculations as 0.01

eV/Å.

Results and Discussions:

Structure of ScS₂ Monolayer:

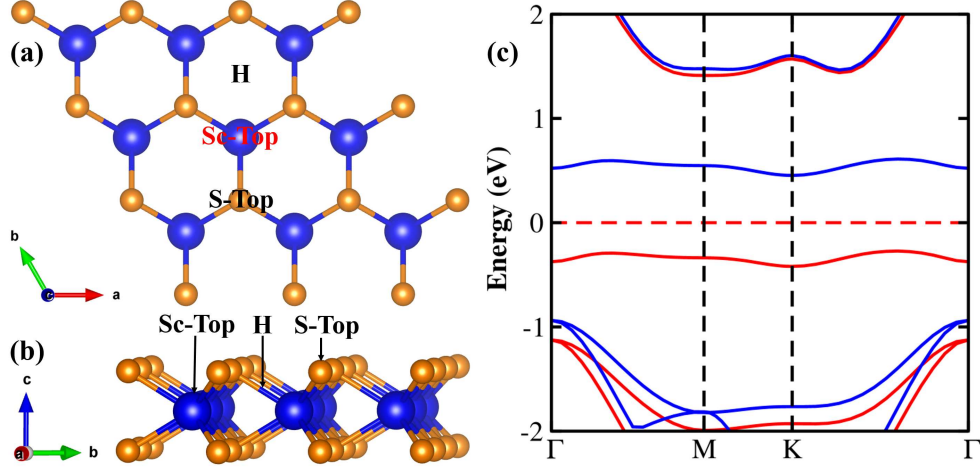


Figure 1: (a) Top-view of the optimized 3X3X1 supercell of ScS₂ monolayer marked with possible adsorption sites (b) side-view of the optimized 3X3X1 supercell of ScS₂ monolayer marked with possible adsorption sites. Blue and orange balls represent Sc and S atoms respectively. (c) Calculated electronic band-structure of H-ScS₂ monolayer. Spin-up states are marked with red and spin-down states are marked with blue colour.

The optimized structure of monolayer ScS₂ is shown in the Figure 1(a) and (b). Here, the structure is two-dimensional and consists of one ScS₂ sheet oriented along the (0, 0, 1) direction consisting one Sc-layer sandwiched between two S-layers. Due to the hexagonal symmetry, each Sc atom occupies the trigonal prismatic centre position by sharing bonds to six equivalent S atoms in the 6-coordinated geometry of the trigonal prism. We obtained the $Sc - S$ bond length and the $\angle S - Sc - S$ bond angle as 2.57Å and $\sim 95^\circ$, respectively. The optimized lattice parameter determined from our calculations (3.79Å) is in good agreement with the previous studies^{22,23}. The electronic band-structure of the optimized H-ScS₂ is shown in the Figure 1(c). We found an indirect bandgap of 0.73 eV which also matches with the previous predictions of 0.74 eV²² and 0.72 eV²³. As the experimental report on the synthesis

of single layer ScS₂ is not available yet to best of our knowledge, the next important step is to theoretically explore the possibility of exfoliation of monolayer of ScS₂ from bulk. For this we calculated the exfoliation energy per atom which is basically the average energy per atom required to remove a layer from it's layered bulk counterpart, using the formula:

$$E_{exf} = \frac{E_{mono}}{N_{mono}} - \frac{E_{bulk}}{N_{bulk}}. \quad (1)$$

Here, E_{mono} and E_{bulk} are the total energies of the monolayer and the bulk materials, respectively, and N_{mono} and N_{bulk} are the number of atoms in the monolayer and in the bulk, respectively. We obtained the value as 150 meV/atom for H-ScS₂ and reporting here for the first time to best of our knowledge. It is well within the desirable limit of 200 meV/atom³², although materials having exfoliation energy as high as 260 meV/atom like Ca₂N³³ and ~600 meV/atom for silicene and GeO, have already been synthesized experimentally. Therefore, it can very well be predicted that the single layer of ScS₂ can be easily exfoliated from its bulk counterpart. The stability of the H-ScS₂ monolayer has already been shown in the previous papers^{22,34}.

Adsorption of the Cations:

Adsorption energy of metal atoms on the electrode material is a crucial parameter in determining the electrochemical performance of cathode or anode. For cathode, a relatively high adsorption energy is expected. To study the metal atoms adsorption on the ScS₂ surface we considered one adatom in a 3×3×1 supercell which is big enough to avoid any interactions between the adsorbates. There are three possible adsorption sites based on the symmetry and chemical environment, namely: (a) H site, (b) Sc-top site and (c) S-top site as marked in the Figure1(a) and (b). The adsorption energies of the cations on these sites were calculated by the formula:

$$E_{ads} = E_{ScS_2M_n} - E_{ScS_2} - nE_M \quad (2)$$

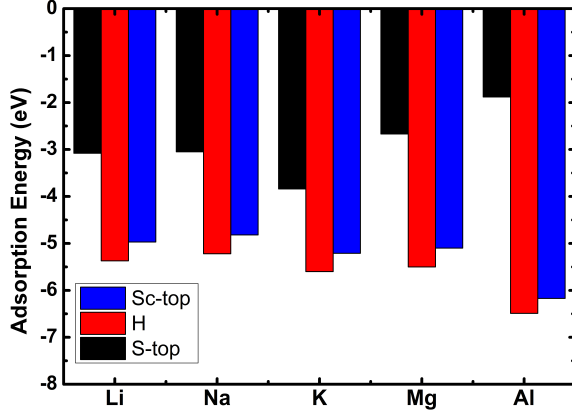


Figure 2: Adsorption energy of different cations on the ScS₂ monolayer surface at different adsorption sites

where, $E_{ScS_2M_n}$ is the total energy of the metal atom(s) adsorbed ScS₂ monolayer, E_{ScS_2} is the total energy of the pristine ScS₂ monolayer, E_M is the energy per atom of the metal cation calculated from the corresponding bulk phase and n is the number of metal atoms adsorbed per ScS₂ formula unit. We considered the bulk bcc (body-centred cubic) structure for Li, Na and K and primitive hexagonal for Mg and fcc (face-centred cubic) for Al to calculate E_M . The calculated adsorption energies of the cations on each of the adsorption sites are shown in the Figure 2. Negative values of the adsorption energy indicate the exothermic interactions between the adsorbent and adsorbates and also signify effective adsorption of all the metal atoms on the ScS₂ monolayer which is not the general case for TMDCs⁴. From the Figure 2 it can be seen that H site is the most favorable adsorption site for all the metal atoms, followed by Sc-top site and S-top site. This can be explained from the fact that generally chemisorbed atoms prefer the high-coordination sites³⁵. The detail explanation is given later on. On comparing the adsorption energies of Li (-5.37 eV), Na (-5.22 eV) and K (-5.6 eV) on ScS₂ to the other cathode materials like ScO₂ (-3.18 eV for Li, -2.87 eV for Na, -9.18 for K)¹⁸, MnO₂ (-2.54 for Li, -2.38 for Na)⁹, CoO₂ (-3.60 for Li, -3.40 for Na)⁹, NiO₂ (-2.17 for Li, -2.56 for Na)⁹, NbS₂ (-2.03 for Li, -1.80 for Na)³⁶ etc. it is found that ScS₂

attracts the alkali metal atoms more strongly which is desirable for cathode materials. It should be noted here that in contrast to our case, for ScO_2 monolayer there is a hexagonal to trigonal phase transition at very low concentration of Li and K adsorption. In fact for the whole range of concentration of the adsorbed metal atoms, no significant structural changes were observed for ScS_2 monolayer which indicates possible electrochemical reversibility of the material. Also for Mg (-5.5 eV) and Al (-6.49 eV), ScS_2 poses higher adsorption energy than other materials like MoS_2 nanoribbon (-4.85 eV for Mg)^{4,21}. We further calculated the binding energy of the metal atoms by the formula:

$$E_{binding} = [E_{\text{ScS}_2\text{M}_n} - E_{\text{ScS}_2} - nE_M]/n \quad (3)$$

which basically is same as Equation 3.2 for $n=1$.

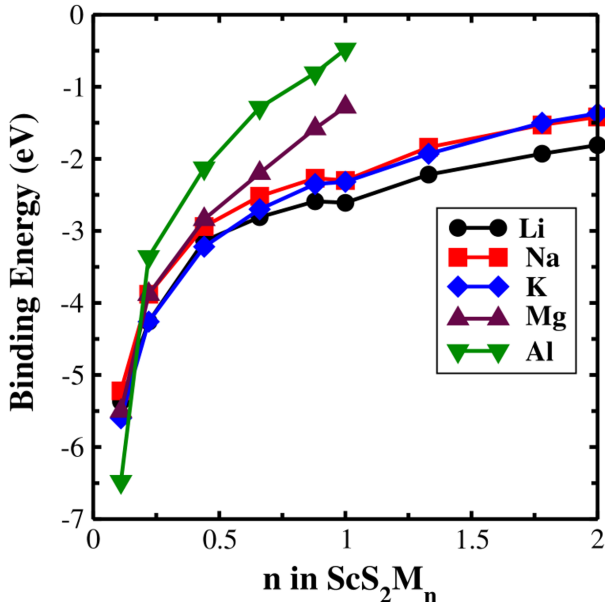


Figure 3: Calculated binding energies for different metals on the ScS_2 surface as a function of metal atom concentration

Figure 3 shows the binding energy as function of ion concentration ($M_n\text{ScS}_2$) in the $3 \times 3 \times 1$ supercell of ScS_2 . The binding energy remains negative for the whole range indicating the metal atoms will prefer to be absorbed on the host material even in higher concentration

rather than forming metal cluster themselves². However, the adsorption energy decays with the increase in the ion concentration due the electrostatic repulsive forces among the ions. As K has the highest ionic radius among the alkali metals studied, the increase in the ion concentration for K results in more electrostatic repulsion, and hence, higher reduction in the binding energy than others.

Table 1: Metal atoms adsorption on the H-site of ScS₂ monolayer: Net Bader charge on different atoms (q_M : Metals atoms, q_S : each of the neighboring three S atoms^a) and the distances of the metal atoms adsorbed in the H site from the neighboring three Sc atoms (D_{M-Sc}) and three S atoms (D_{M-S}) (Figure 1)

Metal Atom (M)	q_M (e)	q_S (e)	D_{M-Sc} (Å)	D_{M-S} (Å)
Li	0.86	-1.14	3.49	2.35
Na	0.78	-0.92	3.89	2.67
K	0.81	-0.89	4.35	3.04
Mg	1.27	-1.03	3.38	2.35
Al	1.47	-0.95	3.16	2.16

^aThe net Bader charge on each of the three neighboring S atoms of the H site in the pristine ScS₂ is -0.74 e

Table 1 shows the different important parameters related to the adsorption of metal adatoms on the ScS₂ surface. As the differences in the electronegativity between S and the metal atoms are quite high than those of the Sc and the metal atoms, the adsorbates are more closely and strongly bonded to the three neighboring S atoms than the Sc atoms as evidenced by the less metal–S distances (D_{M-S}) than the corresponding metal–Sc distances (D_{M-Sc}) given in the Table 1. Due to the stronger electronegativity of S than that of the metal atoms, all the cations act as electron donors. From the Bader charge analysis as given the Table 1 it can be seen that Li, Na, K, Mg and Al donates 0.86e, 0.78e, 0.81e, 1.27e and 1.47e, respectively, to the adsorbent system. On comparing the electron transfer of the Li, Na and K atoms on the FeSe surface and the charge transfer to the Cl atoms in their respective chloride compounds (LiCl, NaCl and KCl)³⁷, we found that these atoms on the ScS₂ monolayer surface can safely be taken as fully ionized, i.e, in the charge state of +1. We also found that, the Mg atom adsorbed on the ScS₂ surface might not get fully ionized (but will be very close to it) as the earlier comparison as well as the study on VS₂

surface⁴ reveals a charge transfer about 1.5e as equivalent to full ionization or charge state of +2. However, Al atom adsorbed in our case, is nowhere close to full ionization (charge state of +3), which can be understood from its relatively higher electronegativity (i.e., lower difference of electronegativity with S) among all the metal atoms considered. As expected, all these electrons from the metal atoms has been transferred to the three neighboring S atoms of the H site as evidenced by the increase of the net Bader charges of these atoms from the pristine ScS₂ (Table 1). Practically metal atoms do not interact directly with Sc atoms but only interact with S atoms which also explains the probable reason of H site being the most favorable adsorption site as in this configuration the metal atoms can maximize the S-coordination number and effectively interact with more no of S atoms than the other configurations.

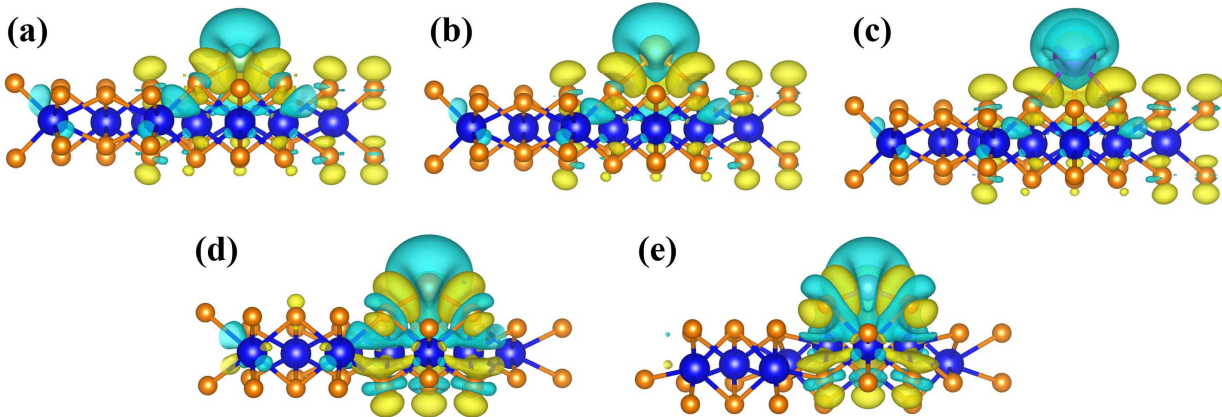


Figure 4: Plot of differential charge density of (a) Li, (b) Na, (c) K, (d) Mg, and (e) Al atom adsorbed on the ScS₂ monolayer. The iso-surface value is taken as $0.0075 \text{ e}/\text{\AA}^3$. Yellow and cyan surfaces represent the charge accumulation and depletion region respectively.

To visualize the nature of the charge transfer process we calculated the differential charge density defined by the formula:

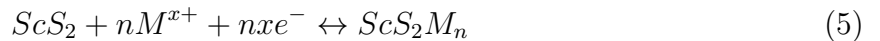
$$\rho_{diff} = \rho_{ScS_2+M}(r) - \rho_{ScS_2}(r) - \rho_M(r) \quad (4)$$

where $\rho_{ScS_2+M}(r)$ is the charge density distribution of the combined system of metal atom adsorbed on ScS₂ monolayer, $\rho_{ScS_2}(r)$ is the charge density of the ScS₂ monolayer, and

$\rho_M(r)$ represents the charge density of the metal atom. Figure 4 depicts the visualization of differential charge density plot of the metal atoms adsorption on the ScS_2 surface. From the figure it can be seen that for alkali metal atoms (Li, Na, K) there are distinct positive (charge depletion) and negative region (charge accumulation) of charge densities located on metal atoms and on neighboring S atoms, respectively, signifying the ionic characteristics of the metal-S bonds which is in accordance to the Bader charge analysis discussed above. For Mg, the situation is more or less same except a small shift of the charge accumulation regions from the vicinity of S atoms towards the Mg atom which may be due to some covalent characteristics of the Mg-S bonds, as discussed earlier too, that the Mg atom adsorbed on the ScS_2 surface is not in the full ionization state but very close to it. However, in case of Al adsorption, the covalent component of the Al-S bonds can be clearly seen from the figure. There are charge accumulation region between the adsorbed Al atom and the S atoms and also alternative depletion and accumulation regions. In accordance to the Bader charge analysis, differential charge density plot also suggest that Al-S bonds are not fully ionic bond like others but, also have major covalent components. It should be also noted that for none of the cases any significant charge accumulation or depletion happens on the Sc atoms which supports the fact that metal atoms interact only with S atoms and not with Sc atoms.

Voltage Profile and Theoretical Capacity:

Open circuit voltage (OCV) and theoretical storage capacity are two crucial parameters to determine the performance of electrode materials. Optimization of these two parameters are also important for designing cathode materials. To study OCV and specific capacity we used a $3 \times 3 \times 1$ supercell of ScS_2 and considered the adsorption on both sides. The charge-discharge process of ScS_2 single layer can be described by the following half-cell reaction *vs* M/M^{x+} as:



Now, depending on this reaction the OCV can be calculated from the difference in total energy of the monolayer before and after adsorption of the metal atoms. Neglecting the volume term ($P\nabla V$) and entropy term ($T\nabla S$) the average OCV (V_{avg}) can be expressed as³⁸:

$$V_{avg} = (E_{ScS_2} + nE_M - E_{ScS_2M_n})/nxe \quad (6)$$

where x is the charge state of fully ionized cations in the electrolyte, i.e., $x = 1$ for Li, Na and K; $x = 2$, for Mg and $x = 3$ for Al.

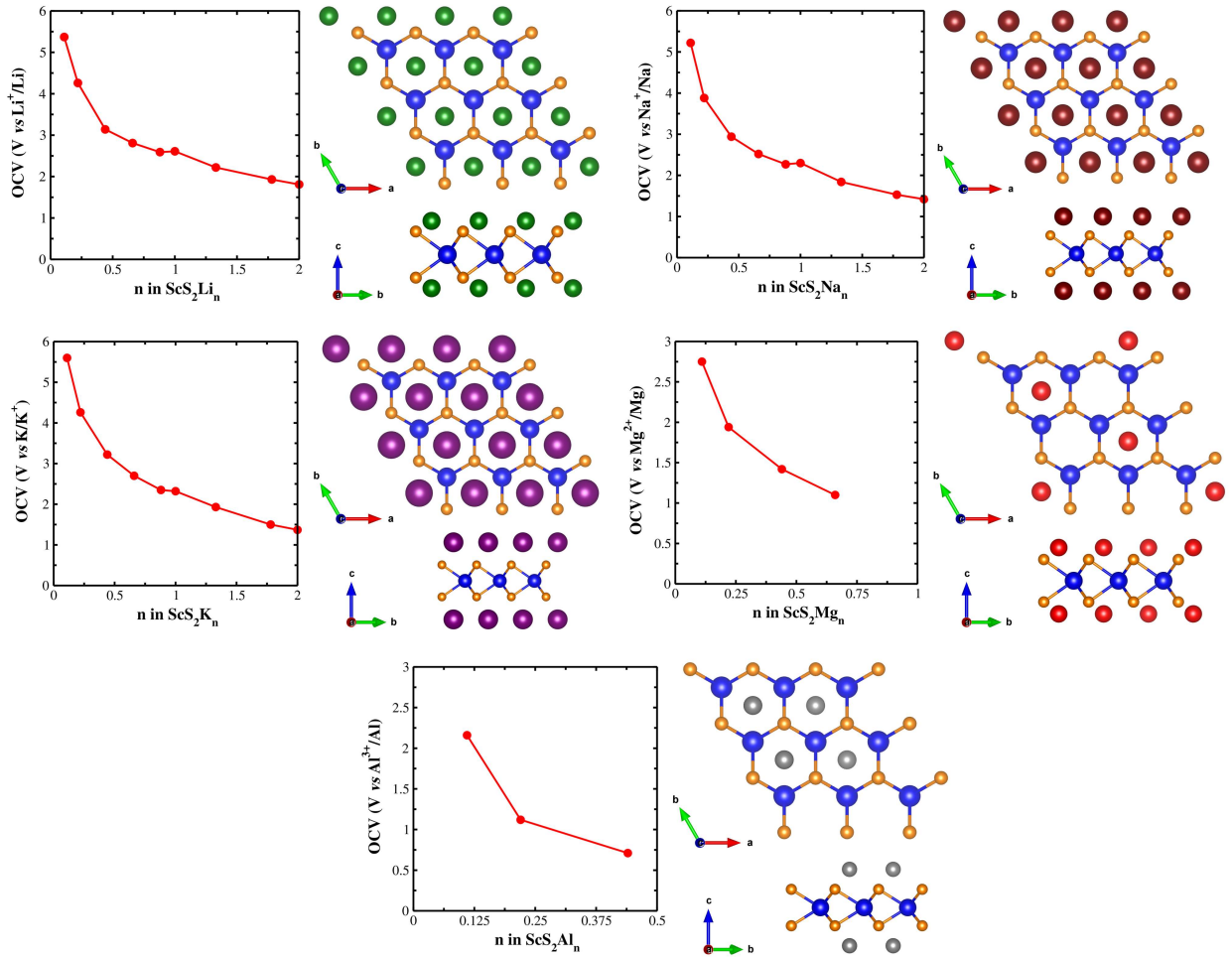


Figure 5: Calculated average cell voltage profile of ScS₂ monolayer and structure with highest no of metal ions absorbed for Li, Na (first row), K, Mg (second row), and Al (third row) adsorption

The calculated average OCV up to fully covered double side adsorption for alkali ions

(M_2ScS_2 ; $M = Li, Na, K$) and partially covered double side adsorption for Mg and Al ions ($MScS_2$; $M = 0.66$ for Mg, 0.44 for Al) has been shown in the Figure 5. The corresponding maximum capacities for different cations have been calculated using the equation:

$$C = nxF/M_{ScS_2} \quad (7)$$

where, F is the Farady constant ($26801 \text{ mA h mol}^{-1}$) and M_{ScS_2} is the molecular weight of ScS_2 ($109.09 \text{ g mol}^{-1}$). The maximum theoretical capacities for the alkali metal ions have been calculated to be $491.36 \text{ mA h g}^{-1}$. At the highest capacity (Li_2ScS_2), the Li-cell voltage is 1.81 V whereas at the concentration of $LiScS_2$, which gives the capacity of $245.68 \text{ mA h g}^{-1}$, the cell voltage remains as high as 2.61 V . For lithiation in ScO_2 , it has been reported to have average OCV as 4.15 V but at the highest capacity of 348 mA h g^{-1} only, and beyond that voltage goes down below 1 V . Also, at the same time a hexagonal to trigonal phase transition¹⁸ takes place which may affects the electrochemical reversibility of the material, as discussed earlier. In fact Liu *et al.* reported the same problem of ScO_2 for Na and K, as well. ScS_2 as LIB cathode is also found to perform well in term of average OCV than MnO_2 ($V_{avg} = 1.11 \text{ V}$ at $308.5 \text{ mA h g}^{-1}$ and 0.98 V at 617 mA h g^{-1})⁹ and similarly to CoO_2 ⁹. On the other hand, V_2O_5 monolayer can deliver specific capacity of $147.40 \text{ mA h g}^{-1}$ (LiV_2O_5) and $294.79 \text{ mA h g}^{-1}$ ($Li_2 V_2O_5$) only for Li at an average OCV of 2.43 V and 2.06 V , respectively¹⁹. Thus, taking into account both the parameters, i.e., OCV and specific capacity, ScS_2 monolayer can be a preferred choice over V_2O_5 monolayer also. In the study of sodiation of NbS_2 ²⁰, Liao *et al.* reported the DFT results for OCV calculations which are found to be in good agreement with experimental results. Inspired from this, we also compared the performance of ScS_2 as LIB cathode with the recent experimentally studied other sulfide materials like 1T-VS₂ or 1T-MoS₂^{39,40} and found ScS_2 to be a better candidate.

Like Li, in case of Na also, ScS_2 performs better than ScO_2 ¹⁸ if the factor of higher capacity and electrochemical reversibility are taken into account as it can deliver the specific

capacity of 245.68 mA h g⁻¹ (NaScS₂) at 2.3 V and 491.36 mA h g⁻¹ (Na₂ScS₂) at 1.42 V without any significant structural change, as shown in Figure 5. It has also found to be a better choice as NIB cathode in term of OCV over oxide layered materials like MnO₂, CoO₂ and NiO₂⁹ which has average OCV of 0.48 V, 0.88 V, and 1.02 V, respectively. V₂O₅ monolayer on the other hand has found to deliver the specific capacity of 147.40 mA h g⁻¹ (NaV₂O₅) at 2.54 V average OCV and 294.79 mA h g⁻¹ (Na₂ V₂O₅) at 1.86 V average OCV which when compared to ScS₂ monolayer it can be seen that for higher capacity at moderate high OCV the later one can be a preferred choice. Recently studied sulfide materials as NIB cathode like NbS₂²⁰ and Cu₂S⁴¹ have been found to have voltage window between 2.75 V to 1 V and specific capacity of 170.66 mA h g⁻¹ and OCV range of 2.6 V to 0.4 V and specific capacity of 294 mA h g⁻¹, respectively, which in every aspect perform poor to ScS₂ monolayer.

As a K-ion battery cathode material, ScS₂ is also found to perform well, delivering the specific capacity of 245.68 mA h g⁻¹ (KScS₂) at an average OCV of 2.32 V and 491.36 mA h g⁻¹ (K₂ScS₂) at 1.37 V. In comparison, V₂O₅ monolayer can only deliver the specific capacity of 147.40 mA h g⁻¹ at slightly higher 2.77 V average OCV¹⁹. Mathew *et al.* have studied the insertion of K-ions in the amorphous iron phosphate and reported a voltage range of 3.5 – 1.5 V with highest capacity around 150 mA h g⁻¹⁴². To compare with their data we also calculated the step potential of K adsorption on ScS₂ using the following equation:

$$V_{step} = \frac{E_{ScS_2M_{n_1}} + (n_2 - n_1)E_M - E_{ScS_2M_{n_2}}}{(n_2 - n_1)xe} \quad (8)$$

where, n₁ and n₂ (n₂>n₁) are the metal ion concentrations in one ScS₂ formula unit in two successive steps. It gives the voltage range of 5.6 – 2.05 V with capacity of 245.68 mA h g⁻¹ at an average OCV of 2.32 V. MoN₂ has been reported to have a theoretical capacity of 432 mA h g⁻¹ at an average OCV of 1.11 V which is again not as good as ScS₂ in terms of both average OCV and specific capacity. Other than these alkali metal ions, 2D ScS₂ has

also been found to perform well as cathode of multivalent cations like Mg and Al in terms of OCV and specific capacity. For Mg, it can deliver maximum of 324.29 mA h g⁻¹ (Mg_{0.66}ScS₂) theoretical capacity at an average OCV of 1.1 V beyond which the step potential becomes negative. For comparison, V₂O₅ monolayer can deliver 294.79 mA h g⁻¹ theoretical capacity at 1.02 V average OCV and its bulk counterpart delivers even less specific capacity of 260 mA h g⁻¹ at OCV 1.83 V¹⁹. On the other hand one of the best known Mg-ion cathode material Mo₆S₈ is known to produce charge-storage capacity of 110 mA h g⁻¹ only at an operating voltage ~1.2 V⁴³. CuS- studied for the same purpose show an average storage capacity ~300 mA h g⁻¹ in the voltage range of 2.4 V to 0 V which can be compared to our step voltage potential range of 2.75 V to 0.44 V⁴³ which is better for the obvious reason. Next, for Al we found ScS₂ monolayer to deliver same theoretical specific capacity of 324.29 mA h g⁻¹ (Al_{0.44}ScS₂) like Mg at an average OCV of 0.71 V. The step potential window in this case in the range of 2.16 V – 0.31 V. To give a context to our findings we compared it with recently studied layered sulfide materials like TiS₂⁴⁴ which experimentally gives a voltage range of ~1.3 V–0.2 V and specific capacity of ~50 mA h g⁻¹ only, MoS₂⁴⁵ delivers specific capacity of 253.6 mA h g⁻¹ with a voltage between 2 V–0.5 V. ScS₂ also predicted to theoretically perform better than other TMDCs that has been studied as Al-ion battery cathode materials like TiO₂ (1.1 V–0.4 V, 75 mA h g⁻¹)⁴⁶, VO₂ (0.9 V–0.01 V, 116 mA h g⁻¹)⁴⁷.

Most of the cathode materials studied so far for metal ion batteries are not able to deliver large specific capacity while holding high OCV. In this context, ScS₂ can be an interesting candidate for cathode material as it maintains a good balance between high operating voltage window and the amount of ions it can hold i.e., the specific capacity.

Diffusion Kinetics:

The diffusion kinetics of the ions in the cathode is directly related to the rate of the charge/discharge process of the rechargeable batteries and hence it is a very crucial pa-

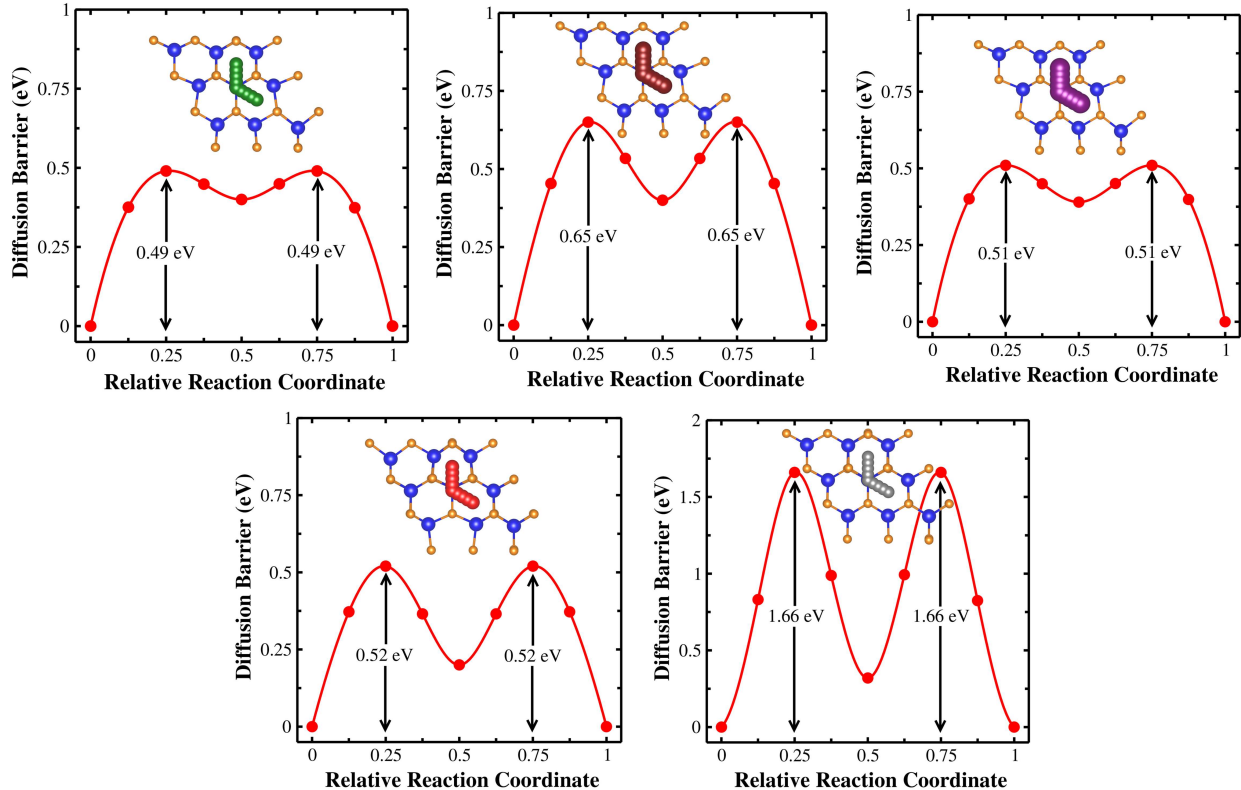


Figure 6: Diffusion barrier profile for the (i) Li, (ii) Na, (iii) K (iv) Mg and (v) Al atoms on the ScS_2 monolayer surface

parameter to study. For this purpose we employed the CI-NEB method³¹ as discussed in the computational details section to find the diffusion barrier height (E_B) and the minimum energy path. From the study of the adsorption of the adatoms on the ScS_2 surface, we have seen that H is the most energetically favorable position followed by Sc-top and S-top sites. Accordingly we have predesigned two diffusion pathways, (i) cations move from one H site to the adjacent H site through a Sc-top site and (ii) cations move from one H site to the another H site in a linear path. Here we did not consider a third possibility of cation diffusion along the path H to H *via* S-top site because of the fact that the adsorption energies at the S-top site are significantly less than the other two sites indicating a higher diffusion barrier which has also been seen for other 2D materials⁴. We considered seven images between the two H sites. After optimization we found that the predesigned path (ii) actually obtained the same pathway as (i), which indicates path (i) to be the probable minimum energy path for

cation diffusion on the ScS₂ surface. The optimized diffusion pathway for the five adatoms are shown in the Figure6. In this *H - Sc - top - H* pathway one metastable state i.e., the local energy minima was found at the Sc-top site for all of the adsorbed cations. Also two saddle points are observed in the middle of the H-Sc-top bridges. The diffusion energy barriers for Li, Na, K, Mg and Al are found to be 0.49 eV, 0.65 eV, 0.51 eV, 0.52 eV and 1.66 eV respectively as shown in the Figure6. For the alkali atoms the diffusion energy barriers are in the order of $E_{B-Li} < E_{B-K} < E_{Na}$, which is also the case for V₂O₅¹⁹ [Ref: V2O5]. The barrier height for Li-atom on the ScS₂ surface is less than the previously reported 2D materials like MoN₂² and TiO₂⁴⁸ for which the respective heights are 0.78eV and 0.65 eV and also from some of the bulk anodes like Si ($E_B=0.62$ eV)⁴⁹ and cathodes like LiFePO₄ ($E_B=0.60$ eV)⁵⁰⁻⁵² and Li₂FeSiO₄ ($E_B=0.91$ eV)⁵³. In case of Na diffusion, the migration barrier is slightly higher than Li on ScS₂ but it's still better than many other electrodes like V₂O₅¹⁹, Na_{0.33}Si₂₄⁵⁴, Si⁴⁹, Ge⁴⁹ etc., the respective barrier heights are 1.17 eV, 0.68eV, 1.08 eV and 0.78 eV. For K-atom migration on the monolayer of ScS₂, the barrier height is almost equal to that of the MoN₂ surface ($E_B=0.49$ eV)² and better than that of the bulk-V₂O₅ ($E_B = 1.66$ eV)¹⁹. We found the Mg diffusion on the ScS₂ more facile than on the surface of TiS₂ ($E_B=0.55$ eV)⁵⁵, V₂O₅ ($E_B=1.36$ eV)¹⁹, and FeSe ($E_B=0.85$ eV)³⁷. Our result is also comparable to the migration energy barrier for Mg on the zigzag MoS₂ nanoribbon surface ($E_B=0.48$ eV)²¹, which has been studied as a promising cathode material for Mg-ion battery. Al has the highest diffusion energy barrier among the five cations we studied. Because of the unavailability of the theoretical results on the same for the cathode materials of the Al-ion battery, it's hard to compare the performance of our material directly to other materials in this aspect. However, the migration barrier for K atom in the bulk of V₂O₅¹⁹ is same as of Al on ScS₂ surface. From the previous discussion on the adsorption of adatoms on the monolayer of ScS₂ we have seen that the Al is not fully ionized and the Al-S bonding has some covalent character unlike other atoms. The adatoms sitting on the H-site have the S coordination number as three. Now in the course of migration from H-site to Sc-top

site, adatoms cross the saddle point which is found to be positioned in the middle of the H–Sc-top bridge which is two-coordinated w.r.t. S atoms. As the covalent bonds are the directional bonds, the difference in coordination number between any two adsorption sites (in this case, between the ground state and the transition state) results in higher change in energy (in this case, the diffusion barrier) than in the case of ionic bonds which are non-directional^{35,56} in nature. The fact that the difference between the adsorption energies on S-top site (one-coordinated w.r.t. S atom) and H-site for Al atom is the highest among all also is in accordance with this argument. So, it may be the reason for Al to have highest diffusion barrier among the studied cations.

From the above discussion on the diffusion kinetics of the five cations on the ScS₂ surface and the comparison with other materials, we can infer that Li, Na, K and Mg can migrate with ease indicating a good charge/discharge performance. However, for Al, the diffusion barrier is high and needs further efforts to minimize it. For example, in case of Li, Guo et al.⁵⁷ shown that the diffusion barrier on phosphorene sheet can be significantly reduced after introducing specific vacancy defects.

References

- (1) Tarascon, J.-M.; Armand, M. Issues and challenges facing rechargeable lithium batteries. *Nature* **2001**, *414*, 359–367.
- (2) Zhang, X.; Yu, Z.; Wang, S.-S.; Guan, S.; Yang, H. Y.; Yao, Y.; Yang, S. A. Theoretical prediction of MoN₂ monolayer as a high capacity electrode material for metal ion batteries. *J. Mater. Chem. A* **2016**, *4*, 15224–15231.
- (3) Xu, B.; Qian, D.; Wang, Z.; Meng, Y. S. Recent progress in cathode materials research for advanced lithium ion batteries. *Mater. Sci. Eng. R Rep* **2012**, *73*, 51–65.
- (4) Wang, D.; Liu, Y.; Meng, X.; Wei, Y.; Zhao, Y.; Pang, Q.; Chen, G. Two-dimensional

- VS₂ monolayers as potential anode materials for lithium-ion batteries and beyond: first-principles calculations. *J. Mater. Chem. A* **2017**, *5*, 21370–21377.
- (5) Goodenough, J. B.; Park, K.-S. The Li-Ion Rechargeable Battery: A Perspective. *J. Am. Chem. Soc.* **2013**, *135*, 1167–1176.
- (6) Okubo, M.; Hosono, E.; Kim, J.; Enomoto, M.; Kojima, N.; Kudo, T.; Zhou, H.; Honma, I. Nanosize Effect on High-Rate Li-Ion Intercalation in LiCoO₂ Electrode. *J. Am. Chem. Soc.* **2007**, *129*, 7444–7452.
- (7) Yuan, L.-X.; Wang, Z.-H.; Zhang, W.-X.; Hu, X.-L.; Chen, J.-T.; Huang, Y.-H.; Goodenough, J. B. Development and challenges of LiFePO₄ cathode material for lithium-ion batteries. *Energy Environ. Sci.* **2011**, *4*, 269–284.
- (8) Xiang, X.; Zhang, K.; Chen, J. Recent Advances and Prospects of Cathode Materials for Sodium-Ion Batteries. *Adv. Mater.* **2015**, *27*, 5343–5364.
- (9) Leong, C. C.; Pan, H.; Ho, S. K. Two-dimensional transition-metal oxide monolayers as cathode materials for Li and Na ion batteries. *Phys. Chem. Chem. Phys.* **2016**, *18*, 7527–7534.
- (10) Raccichini, R.; Varzi, A.; Wei, D.; Passerini, S. Critical Insight into the Relentless Progression Toward Graphene and Graphene-Containing Materials for Lithium-Ion Battery Anodes. *Adv. Mater.* **2017**, *29*, 1603421.
- (11) Zhuang, J.; Xu, X.; Peleckis, G.; Hao, W.; Dou, S. X.; Du, Y. Silicene: A Promising Anode for Lithium-Ion Batteries. *Adv. Mater.* **2017**, *29*, 1606716.
- (12) Zhu, J.; Chroneos, A.; Schwingenschlogl, U. Silicene/germanene on MgX₂ (X = Cl, Br, and I) for Li-ion battery applications. *Nanoscale* **2016**, *8*, 7272–7277.
- (13) Rao, D.; Zhang, L.; Meng, Z.; Zhang, X.; Wang, Y.; Qiao, G.; Shen, X.; Xia, H.; Liu, J.;

- Lu, R. Ultrahigh energy storage and ultrafast ion diffusion in borophene-based anodes for rechargeable metal ion batteries. *J. Mater. Chem. A* **2017**, *5*, 2328–2338.
- (14) Li, W.; Yang, Y.; Zhang, G.; Zhang, Y.-W. Ultrafast and Directional Diffusion of Lithium in Phosphorene for High-Performance Lithium-Ion Battery. *Nano Lett.* **2015**, *15*, 1691–1697.
- (15) Sibari, A.; Marjaoui, A.; Lakhal, M.; Kerrami, Z.; Kara, A.; Benaissa, M.; Ennaoui, A.; Hamedoun, M.; Benyoussef, A.; Mounkachi, O. Phosphorene as a promising anode material for (Li/Na/Mg)-ion batteries: A first-principle study. *Sol. Energy Mater. Sol. Cells* **2018**, *180*, 253–257.
- (16) Hu, J.; Xu, B.; Yang, S. A.; Guan, S.; Ouyang, C.; Yao, Y. 2D Electrides as Promising Anode Materials for Na-Ion Batteries from First-Principles Study. *ACS Appl. Mater. Interfaces* **2015**, *7*, 24016–24022.
- (17) Kumar, P.; Abuhimd, H.; Wahyudi, W.; Li, M.; Ming, J.; Li, L.-J. Review—Two-Dimensional Layered Materials for Energy Storage Applications. *ECS J. Solid State Sci. Technol.* **2016**, *5*, Q3021–Q3025.
- (18) Liu, Z.; Deng, H.; Zhang, S.; Hu, W.; Gao, F. A first-principles investigation of the ScO₂ monolayer as the cathode material for alkali metal-ion batteries. *J. Mater. Chem. A* **2018**, *6*, 3171–3180.
- (19) Zhao, X.; Zhang, X.; Wu, D.; Zhang, H.; Ding, F.; Zhou, Z. Ab initio investigations on bulk and monolayer V₂O₅ as cathode materials for Li-, Na-, K- and Mg-ion batteries. *J. Mater. Chem. A* **2016**, *4*, 16606–16611.
- (20) Liao, Y.; Park, K.-S.; Xiao, P.; Henkelman, G.; Li, W.; Goodenough, J. B. Sodium Intercalation Behavior of Layered Na_xNbS₂ (0 ≤ x ≤ 1). *Chem. Mater.* **2013**, *25*, 1699–1705.

- (21) Yang, S.; Li, D.; Zhang, T.; Tao, Z.; Chen, J. First-Principles Study of Zigzag MoS₂ Nanoribbon As a Promising Cathode Material for Rechargeable Mg Batteries. *J. Phys. Chem. C* **2012**, *116*, 1307–1312.
- (22) Zhang, H.; Lin, X.; Tang, Z.-K. Stable ScS₂ nanostructures with tunable electronic and magnetic properties. *Solid State Commun.* **2015**, *220*, 12–16.
- (23) Reyes-Retana, J. A.; Cervantes-Sodi, F. Spin-orbital effects in metal-dichalcogenide semiconducting monolayers. *Sci. Rep.* **2016**, *6*, 24093.
- (24) Kresse, G.; Hafner, J. Ab initio Molecular Dynamics for Liquid metals. *Phys. Rev. B* **1993**, *47*, 558–561.
- (25) Kresse, G.; Furthmüller, J. Efficiency of Ab-initio Total Energy Calculations for Metals and Semiconductors using a Plane-wave Basis Set. *Comput. Mater. Sci.* **1996**, *6*, 15–50.
- (26) Kresse, G.; Furthmüller, J. Efficient Iterative Schemes for Ab initio Total-energy Calculations using a Plane-wave Basis Set. *Phys. Rev. B* **1996**, *54*, 11169–11186.
- (27) Blüchl, P. E. Projector augmented-wave method. *Phys. Rev. B* **1994**, *50*, 17953–17979.
- (28) Perdew, J. P.; Burke, K.; Ernzerhof, M. Generalized Gradient Approximation Made Simple. *Phys. Rev. Lett.* **1996**, *77*, 3865–3868.
- (29) Grimme, S.; Antony, J.; Ehrlich, S.; Krieg, H. A consistent and accurate ab initio parametrization of density functional dispersion correction (DFT-D) for the 94 elements H-Pu. *J. Chem. Phys.* **2010**, *132*, 154104.
- (30) Monkhorst, H. J.; Pack, J. D. Special points for Brillouin-zone integrations. *Phys. Rev. B* **1976**, *13*, 5188–5192.
- (31) Henkelman, G.; Uberuaga, B. P.; Jonsson, H. A climbing image nudged elastic band method for finding saddle points and minimum energy paths. *J. Chem. Phys.* **2000**, *113*, 9901–9904.

- (32) Choudhary, K.; Garrity, K. F.; Reid, A. C. E.; DeCost, B.; Biacchi, A. J.; Hight Walker, A. R.; Trautt, Z.; Hattrick-Simpers, J.; Kusne, A. G.; Centrone, A. et al. The joint automated repository for various integrated simulations (JARVIS) for data-driven materials design. *npj Comput. Mater.* **2020**, *6*, 173.
- (33) Zhou, J.; Shen, L.; Costa, M. D.; Persson, K. A.; Ong, S. P.; Huck, P.; Lu, Y.; Ma, X.; Chen, Y.; Tang, H. et al. 2D MatPedia, an open computational database of two-dimensional materials from top-down and bottom-up approaches. *Sci. Data* **2019**, *6*, 86.
- (34) Ataca, C.; Aahin, H.; Ciraci, S. Stable, Single-Layer MX₂ Transition-Metal Oxides and Dichalcogenides in a Honeycomb-Like Structure. *J. Phys. Chem. C* **2012**, *116*, 8983–8999.
- (35) Diehl, R. D.; McGrath, R. Current progress in understanding alkali metal adsorption on metal surfaces. *J. Phys.: Condens. Matter* **1997**, *9*, 951–968.
- (36) Zhu, J.; Alshareef, H. N.; Schwingenschlogl, U. Functionalized NbS₂ as cathode for Li- and Na-ion batteries. *Appl. Phys. Lett.* **2017**, *111*, 043903.
- (37) Lv, X.; Li, F.; Gong, J.; Gu, J.; Lin, S.; Chen, Z. Metallic FeSe monolayer as an anode material for Li and non-Li ion batteries: a DFT study. *Phys. Chem. Chem. Phys.* **2020**, *22*, 8902–8912.
- (38) Aydinol, M. K.; Kohan, A. F.; Ceder, G.; Cho, K.; Joannopoulos, J. Ab initio study of lithium intercalation in metal oxides and metal dichalcogenides. *Phys. Rev. B* **1997**, *56*, 1354–1365.
- (39) Liang, X.; Chen, M.; Zhu, H.; Zhu, H.; Cui, X.; Yan, J.; Chen, Q.; Xia, X.; Liu, Q. Unveiling the solid-solution charge storage mechanism in 1T vanadium disulfide nanoarray cathodes. *J. Mater. Chem. A* **2020**, *8*, 9068–9076.

- (40) Wu, M.; Zhan, J.; Wu, K.; Li, Z.; Wang, L.; Geng, B.; Wang, L.; Pan, D. Metallic 1T MoS₂ nanosheet arrays vertically grown on activated carbon fiber cloth for enhanced Li-ion storage performance. *J. Mater. Chem. A* **2017**, *5*, 14061–14069.
- (41) Kim, J.-S.; Kim, D.-Y.; Cho, G.-B.; Nam, T.-H.; Kim, K.-W.; Ryu, H.-S.; Ahn, J.-H.; Ahn, H.-J. The electrochemical properties of copper sulfide as cathode material for rechargeable sodium cell at room temperature. *J. Power Sources* **2009**, *189*, 864–868.
- (42) Mathew, V.; Kim, S.; Kang, J.; Gim, J.; Song, J.; Baboo, J. P.; Park, W.; Ahn, D.; Han, J.; Gu, L. et al. Amorphous iron phosphate: potential host for various charge carrier ions. *NPG Asia Mater.* **2014**, *6*, e138–e138.
- (43) Kravchyk, K. V.; Widmer, R.; Erni, R.; Dubey, R. J.-C.; Krumeich, F.; Kovalenko, M. V.; Bodnarchuk, M. I. Copper sulfide nanoparticles as high-performance cathode materials for Mg-ion batteries. *Sci. Rep.* **2019**, *9*, 7988.
- (44) Geng, L.; Scheifers, J. P.; Fu, C.; Zhang, J.; Fokwa, B. P. T.; Guo, J. Titanium Sulfides as Intercalation-Type Cathode Materials for Rechargeable Aluminum Batteries. *ACS Appl. Mater. Interfaces* **2017**, *9*, 21251–21257.
- (45) Li, Z.; Niu, B.; Liu, J.; Li, J.; Kang, F. Rechargeable Aluminum-Ion Battery Based on MoS₂ Microsphere Cathode. *ACS Appl. Mater. Interfaces* **2018**, *10*, 9451–9459.
- (46) Liu, S.; Hu, J. J.; Yan, N. F.; Pan, G. L.; Li, G. R.; Gao, X. P. Aluminum storage behavior of anatase TiO₂ nanotube arrays in aqueous solution for aluminum ion batteries. *Energy Environ. Sci.* **2012**, *5*, 9743–9746.
- (47) Wang, W.; Jiang, B.; Xiong, W.; Sun, H.; Lin, Z.; Hu, L.; Tu, J.; Hou, J.; Zhu, H.; Jiao, S. A new cathode material for super-valent battery based on aluminium ion intercalation and deintercalation. *Sci. Rep.* **2013**, *3*, 3383.

- (48) Yang, Z.; Choi, D.; Kerisit, S.; Rosso, K. M.; Wang, D.; Zhang, J.; Graff, G.; Liu, J. Nanostructures and lithium electrochemical reactivity of lithium titanites and titanium oxides: A review. *J. Power Sources* **2009**, *192*, 588–598.
- (49) Chou, C.-Y.; Lee, M.; Hwang, G. S. A Comparative First-Principles Study on Sodiation of Silicon, Germanium, and Tin for Sodium-Ion Batteries. *J. Phys. Chem. C* **2015**, *119*, 14843–14850.
- (50) Islam, M. S.; Driscoll, D. J.; Fisher, C. A. J.; Slater, P. R. Atomic-Scale Investigation of Defects, Dopants, and Lithium Transport in the LiFePO_4 Olivine-Type Battery Material. *Chem. Mater.* **2005**, *17*, 5085–5092.
- (51) Gardiner, G. R.; Islam, M. S. Anti-Site Defects and Ion Migration in the $\text{LiFe}_{0.5}\text{Mn}_{0.5}\text{PO}_4$ Mixed-Metal Cathode Material. *Chem. Mater.* **2010**, *22*, 1242–1248.
- (52) Fisher, C. A. J.; Hart Prieto, V. M.; Islam, M. S. Lithium Battery Materials LiMPO_4 ($\text{M} = \text{Mn}, \text{Fe}, \text{Co}, \text{and Ni}$): Insights into Defect Association, Transport Mechanisms, and Doping Behavior. *Chem. Mater.* **2008**, *20*, 5907–5915.
- (53) Armstrong, A. R.; Kuganathan, N.; Islam, M. S.; Bruce, P. G. Structure and Lithium Transport Pathways in $\text{Li}_2\text{FeSiO}_4$ Cathodes for Lithium Batteries. *J. Am. Chem. Soc.* **2011**, *133*, 13031–13035.
- (54) Arrieta, U.; Katcho, N. A.; Arcelus, O.; Carrasco, J. First-Principles Study of Sodium Intercalation in Crystalline $\text{Na}_x\text{Si}_2\text{O}_7$ ($0 \leq x \leq 4$) as Anode Material for Na-ion Batteries. *Sci. Rep.* **2017**, *7*, 5350.
- (55) Samad, A.; Shafique, A.; Shin, Y.-H. Adsorption and diffusion of mono, di, and trivalent ions on two-dimensional TiS_2 . *Nanotechnology* **2017**, *28*, 175401.
- (56) Koch, D.; Kulish, V. V.; Manzhos, S. A first-principles study of potassium insertion in

crystalline vanadium oxide phases as possible potassium-ion battery cathode materials. *MRS Commun.* **2017**, *7*, 819–825.

- (57) Guo, G.-C.; Wei, X.-L.; Wang, D.; Luo, Y.; Liu, L.-M. Pristine and defect-containing phosphorene as promising anode materials for rechargeable Li batteries. *J. Mater. Chem. A* **2015**, *3*, 11246–11252.